Available online at www.sciencedirect.com

ScienceDirect

Geochimica et Cosmochimica Acta 221 (2018) 342–357

Geochimica et Cosmochimica Acta

www.elsevier.com/locate/gca

In situ ^{60}Fe-^{60}Ni systematics of chondrules from unequilibrated ordinary chondrites

Myriam Telus [a,b,*], Gary R. Huss [b], Kazuhide Nagashima [b], Ryan C. Ogliore [b,1], Shogo Tachibana [c]

[a] *Geology and Geophysics, School of Ocean, Earth Science and Technology, University of Hawai'i at Mānoa, Honolulu, HI 96822, USA*
[b] *Hawai'i Institute of Geophysics and Planetology, School of Ocean, Earth Science and Technology, University of Hawai'i at Mānoa, Honolulu, HI 96822, USA*
[c] *Department of Natural History Sciences, Hokkaido University, N10 W8, Sapporo 060-0810, Japan*

Received 29 February 2016; accepted in revised form 3 June 2017; available online 12 June 2017

Abstract

The initial ^{60}Fe/^{56}Fe of chondrules from unequilibrated ordinary chondrites (UOCs) can potentially constrain the stellar source of short-lived radionuclides and develop the ^{60}Fe-^{60}Ni ($t_{1/2} = 2.6$ Ma) system for early solar system chronology. However, progress with the ^{60}Fe-^{60}Ni system has been hindered by discrepancies between initial ratios inferred from bulk and *in situ* Fe-Ni analyses. Telus et al. (2016) show that discrepancies between these different techniques stem from late-stage open-system Fe-Ni mobilization. Here, we report *in situ* analyses of the Fe-Ni isotopic composition of ferromagnesian silicates in chondrules from UOCs using the ion microprobe. Of the 24 chondrules analyzed for this study, a few chondrules have resolved excesses in ^{60}Ni of up to 70‰; however, the correlations with Fe/Ni are weak. Although complications from Fe-Ni redistribution make it difficult to interpret the data, we show that the initial ^{60}Fe/^{56}Fe for UOC chondrules is between 5×10^{-8} and 3.0×10^{-7}. This is consistent with a late supernova source for ^{60}Fe, but self-enrichment of the molecular cloud is another possible mechanism for incorporating ^{60}Fe in the solar system. Discrepancies between bulk and *in situ* analyses remain, but likely stem from late-stage open-system Fe-Ni mobilization.

Keywords: ^{60}Fe; Radionuclides; Chondrules; Ion microprobe; Ordinary chondrites

1. INTRODUCTION

The ^{60}Fe-^{60}Ni short-lived radionuclide system ($t_{1/2} = 2.6$ Ma) has been of interest in cosmochemistry and astrophysics for several reasons, including its potential for constraining early solar system chronology (e.g., Shukolyukov and Lugmair, 1993a; Tang and Dauphas, 2012a), its potential as a heat source for planetary differentiation (e.g., Moskovitz and Gaidos, 2011), identifying the stellar source of short-lived radionuclides (e.g., Huss et al., 2009), and understanding the environmental conditions surrounding the Sun's formation (e.g., Hester and Desch, 2005). The presence of live ^{60}Fe in the early solar system has been inferred through excesses in ^{60}Ni that correlate with Fe/Ni in various meteorites (e.g., Shukolyukov and Lugmair, 1993a; Tachibana et al., 2006; Tang and Dauphas, 2012a; Mishra and Goswami, 2014). The initial ^{60}Fe/^{56}Fe for each sample, $(^{60}Fe/^{56}Fe)_0$, is determined from an evolution diagram, which plots the Ni-isotopic composition as a function of the Fe/Ni. The slope of the correlation line gives $(^{60}Fe/^{56}Fe)_0$, which can then be used to constrain

* Corresponding author at: Earth and Planetary Sciences, University of California Santa Cruz, Santa Cruz, CA 95064, USA.
E-mail address: mtelus@ucsc.edu (M. Telus).
[1] Present address: Department of Physics, Washington University in St. Louis, St. Louis, MO 63130, USA.

http://dx.doi.org/10.1016/j.gca.2017.06.013
0016-7037/

the initial solar system $^{60}Fe/^{56}Fe$ value, $(^{60}Fe/^{56}Fe)_{SS}$, as long as the age of the sample has been determined independently, the Fe-Ni system has remained closed, and ^{60}Fe was homogeneously distributed in the solar system. The last two criteria are often assumed.

Progress with using the ^{60}Fe-^{60}Ni system for early solar system chronology or for constraining astrophysical models has been hindered by discrepancies between initial ratios inferred from bulk and *in situ* Fe-Ni analyses. Bulk Fe-Ni analyses of calcium-aluminum-rich inclusions (CAIs), the first solids to form in the solar system, carried out by Birck and Lugmair (1988), found excesses of ^{60}Ni in several inclusions consistent with an initial $(^{60}Fe/^{56}Fe)_{SS}$ of $<1.6 \times 10^{-6}$. However, since CAIs preserve Ni-isotope anomalies, it is not clear whether the excesses in ^{60}Ni are from the decay of ^{60}Fe or simply inherited isotope anomalies, which are common in CAIs. Further application of CAIs to constrain the $(^{60}Fe/^{56}Fe)_{SS}$ has been problematic for this reason. Whole rock analyses of eucrites, basaltic achondrites, by Shukolyukov and Lugmair (1993a, 1993b) show resolved ^{60}Ni excesses that correlate with Fe/Ni. The initial $^{60}Fe/^{56}Fe$ inferred for eucrites Juvinas and Chervony Kut were 4.3×10^{-10} and 3.9×10^{-9}, respectively, implying an 8.3 Ma difference in the crystallization ages of these meteorites (using the 2.6 Ma half-life determined by Rugel et al., 2009). However, internal isochrons from analyses of mineral separates do not show a tight correlation between excess ^{60}Ni and Fe/Ni, indicating the Fe-Ni system did not remain closed for these samples and has been affected by thermal metamorphism (Shukolyukov and Lugmair, 1993a; Quitté et al., 2011). Whole rock analyses of eucrites and diogenites by Tang and Dauphas (2012a) infer an $^{60}Fe/^{56}Fe$ of 3.5×10^{-9} at the end of mantle differentiation of the HED (howardite-eucrite-diogenite) parent body. Using ^{53}Mn-^{53}Cr systematics to infer the time of differentiation, the estimated initial solar system $^{60}Fe/^{56}Fe$ ratio, $(^{60}Fe/^{56}Fe)_{SS}$, is 1.0×10^{-8}. This is also consistent with initial ratios inferred from bulk analyses of angrites (Quitté et al., 2010; Spivak-Birndorf et al., 2011; Tang and Dauphas, 2012a, 2012b). Bulk analyses of chondrules from unequilibrated ordinary chondrites have also been used to help constrain $(^{60}Fe/^{56}Fe)_{SS}$. Excesses in ^{60}Ni are unresolved from zero for most bulk chondrules analyses (Tang and Dauphas, 2012a; Spivak-Birndorf et al., 2012a; Spivak-Birndorf et al., 2012b; Chen et al., 2013); however, recent analyses found resolved excess ^{60}Ni in one Semarkona chondrule (Tang and Dauphas, 2015). The $(^{60}Fe/^{56}Fe)_{SS}$ ratios inferred from bulk chondrule analyses are all consistent with $<3 \times 10^{-8}$. An initial ratio at this level is more consistent with ^{60}Fe being inherited from the galactic background (i.e., material from the interstellar medium inherited by the Sun's molecular cloud; Huss et al., 2009), and would be an insignificant source of heat for planetary differentiation (Moskovitz and Gaidos, 2011).

Initial ratios inferred from *in situ* Fe-Ni analyses often paint a different picture. Kita et al. (2000) analyzed olivine from one Semarkona chondrule, but did not observe resolved excesses in ^{60}Ni. However, subsequent *in situ* analyses of troilite in unequilibrated ordinary chondrites (UOCs) by Tachibana and Huss (2003) found excess ^{60}Ni that correlated with the Fe/Ni ratios. They inferred $(^{60}Fe/^{56}Fe)_0$ for sulfides from Bishunpur and Krymka of $(1–2) \times 10^{-7}$, an order of magnitude higher than initial ratios inferred from bulk analyses. Mostefauoi et al. (2005) analyzed troilite and magnetite from Semarkona and inferred an even higher initial ratio for sulfides of 1×10^{-6}. However, because sulfides are easily altered by mild thermal metamorphism (Guan et al., 2004, 2007) researchers later shifted their gaze to Fe-rich silicates, olivine and pyroxene. Tachibana et al. (2006) infer initial ratios of $(2–3) \times 10^{-7}$ from *in situ* analyses of Semarkona and Bishunpur chondrules, while Mishra et al. (2010) inferred higher initial ratios of up to 6×10^{-7} from similar analyses. However, Telus et al. (2012) show that the high initial ratios inferred from most of the previous *in situ* Fe-Ni analyses are artifacts from the way the isotope ratios were calculated. Isotope ratios calculated from counting data have a positive bias, and the bias is inversely proportional to the number of counts in the denominator of the ratio (Ogliore et al., 2011). The low Ni contents of our samples can potentially lead to significant ratio bias. The bias was accentuated in the early work because the final isotope ratios were calculated from the mean of ratios of a large number of measurement cycles. When the isotope ratios from various studies (Tachibana and Huss, 2003; Guan et al. 2007; Tachibana et al., 2006; Tachibana et al., 2007; Tachibana et al., 2009; Telus et al., 2011) were calculated using total counts and bias was suppressed, evidence for ^{60}Fe disappeared for sulfides and most chondrules (Telus et al., 2012). Nevertheless, evidence for ^{60}Fe in some chondrules remains, with inferred initial ratios ranging from 2×10^{-7} (Telus et al., 2012) to 1×10^{-6} (Mishra and Goswami, 2014; Mishra and Chaussidon 2014), though the isochrons are often not well constrained. The presence of ^{60}Fe at this abundance in the early solar system is consistent with a recent supernova injection of ^{60}Fe and possibly other short-lived radionuclides in the solar system (Hester and Desch, 2005; Huss et al., 2009; Ouellette et al., 2009; Mishra and Goswami, 2014), although an AGB star of >5 solar masses could also potentially provide sufficient ^{60}Fe (Wasserburg et al., 2006). Also, an abundance of this magnitude would have important implications for planetary differentiation models (Moskovitz and Gaidos, 2011).

Here, we present ^{60}Fe-^{60}Ni isotopic data for ferromagnesian silicates in chondrules from unequilibrated ordinary chondrites (UOCs) determined *in situ* using the ion microprobe at the University of Hawai'i. In interpreting these data, we take into account the clear evidence for late-stage redistribution of Fe and Ni in these chondrules, as demonstrated by synchrotron X-ray fluorescence studies (Telus et al., 2016). We find that most chondrules do not show resolved excesses of ^{60}Ni. Some chondrules have resolved excesses in ^{60}Ni, and some measured excesses are large (up to ~70‰). Model isochrons constructed for these chondrules typically show a weak correlation between excess ^{60}Ni and Fe/Ni, indicating that secondary processing disturbed the Fe and Ni isotopic system. Despite this, these chondrules provide useful constraints on the upper and lower limits of the initial $^{60}Fe/^{56}Fe$ of the Solar System.

2. METHODS

2.1. Sample selection

We analyzed olivine and pyroxene from chondrules in the unequilibrated ordinary chondrites Semarkona (LL3.00), QUE97008 (L3.05), EET90161 (L3.05), Bishunpur (LL3.1) and Krymka (LL3.2). We analyzed a wide variety of chondrules (Type I, Type II, cryptocrystalline, barred and porphyritic), but most of the chondrules are Type II porphyritic chondrules. Our primary selection criteria were for chondrules with high enough Fe/Ni to permit us to resolve excess ^{60}Ni and grains large enough to accommodate the ion probe pits. At first, we scanned for suitable chondrules using the electron microprobe (JEOL JXA-8500F) at the University of Hawai'i (UH). We carried out spot analyses with a 10 μm, 200 nA beam at 20 keV to help constrain Fe/Ni. However, the Fe/Ni ratios were often difficult to constrain because the Ni content in the pyroxene grains are generally below the detection limit of the electron probe. Therefore, we turned to using the ion probe for a second scan of suitable chondrules that passed the electron probe screening. We simply checked the Fe/Ni ratio on a few areas of each chondrule using a 3 nA $^{16}O^-$ on the Cameca ims 1280 ion microprobe at UH. This method provided more accurate constraints on Fe/Ni.

We focused most of our efforts on chondrule pyroxenes from UOCs because pyroxenes have high ^{56}Fe/^{62}Ni (e.g., $>2 \times 10^5$) and are less susceptible to thermal metamorphism compared to olivine and sulfides. Also, UOCs of petrologic types 3.00–3.2 have experienced relatively low metamorphic peak temperatures (<400 °C; Huss and Lewis, 1994). Despite all these benefits, X-ray fluorescence maps in Telus et al. (2016) show that Fe and Ni are mobile in UOCs along chondrule fractures. These fractures are often too fine for us to notice or avoid or they are subsurface features we cannot readily detect with the electron probe or ion probe. Therefore, we also carried out X-ray fluorescence mapping at the Australian Synchrotron and the Advanced Photon Source to scan for suitable chondrules that do not show evidence for Fe or Ni mobilization, along with having large grain sizes and high Fe/Ni. Our best chondrules from this survey are SMK1805 chT and SMK312B chQ from Semarkona, a type 3.00 ordinary chondrite. These chondrules met every criterion mentioned above except that they show evidence for Fe mobilization along chondrule fractures. We did not find chondrules that meet every criterion. Finding suitable chondrules for SIMS Fe-Ni analyses is challenging, which may limit its use for constraining the initial $(^{60}Fe/^{56}Fe)_{SS}$.

2.2. Secondary ion mass spectrometry

The UOC chondrules were measured using the Cameca ims 1280 ion microprobe at the University of Hawai'i (UH). Iron and Ni isotopes were measured as positive ions using a 3–10 nA $^{16}O^-$ beam, rastered over 15 μm. Spot sizes ranged from 20 to 40 μm and spots were presputtered (180 s) to minimize surface contamination. The secondary-ion beam was automatically centered in the field aperture using the dynamic transfer deflectors at the beginning of each measurement. Terrestrial standards (San Carlos olivine, San Carlos pyroxene, and hypersthene) were generally measured using lower beam currents (1–3 nA) because of their higher Ni contents. We also used synthetic pyroxene standards, JHpx1 and JHpx2 made in the Volcanology and Experimental Petrology lab at UH (see on-line supplementary information). We used two basic SIMS protocols: monocollection and multicollection.

Monocollection: Nickel ions ($^{60}Ni^+$, $^{61}Ni^+$, and $^{62}Ni^+$) were counted sequentially on the monocollector electron multiplier, while the Fe ions ($^{56}Fe^+$ or $^{57}Fe^+$) were counted on the multicollector Faraday cup (L1) together with ^{60}Ni. The main advantage to using monocollection mode is that the monocollector electron multiplier is large and stable, meaning that changes in the gain of the detector over an analytical session are negligible. Also, any changes in the efficiency of the electron multiplier are cancelled out by taking ratios. The electron multiplier can easily handle all Ni count rates that we encountered (up to 5×10^4 cps; typical count rates ranging from 100 to 1000 cps). The disadvantage is that measurement times are longer since each isotope is counted separately, and fluctuation of secondary ion beam intensity either due to primary beam instability or heterogeneity of Ni contents introduces additional uncertainties in measured Ni isotope ratios. For our most recent monocollection analyses, $^{60}Ni^+$, $^{61}Ni^+$, and $^{62}Ni^+$ were counted for 2, 50, and 10 s, respectively. Thus, each cycle for monocollection required at least 64 s (not including the time necessary to switch between the different masses and time for mass calibration and energy scans). Mass calibration was done automatically every 25 cycles, and energy scans were done every 50 cycles in order to account for sample charging. A typical measurement of 100 cycles lasted 2 hours.

Multicollection: In most cases, Fe and Ni ions were measured simultaneously, with $^{60}Ni^+$, $^{61}Ni^+$, and $^{62}Ni^+$ counted on electron multipliers and $^{56}Fe^+$ measured on a Faraday cup. Sometimes, we set Ni and Fe on separate B-fields and jumped from one to the other. This minimizes the effects of off-axis aberrations and gives the multicollector electron multipliers a rest every cycle. Mass calibration and energy scans were done automatically every 50 cycles. Each measurement cycle lasted 30 seconds and a measurement consisted of 200 cycles; a typical measurement lasted 2 hours. The multicollector electron multipliers are less stable with the gains changing throughout the analytical session (average ^{60}Ni/^{62}Ni ratio change of ~10‰), especially if they have been bombarded with high counts from Ni-rich phases. Unlike monocollection measurements, the gain changes among multicollection electron multipliers introduce inaccuracy in Ni isotope ratios; thus, a correction for drift in the gain of the detectors must be made using standard-sample bracketing. Chondrules BM80 ch37 and QUE ch3 were measured in both monocollection and multicollection mode (Table 1).

The gain of the multicollection electron multipliers degrades quickly during a series of measurements. For this study, we checked the pulse height distribution and adjusted the voltage on the electron multipliers in order

Table 1
Inferred initial $^{60}Fe/^{56}Fe$ ratios for UOC chondrules from ^{62}Ni normalized ratios determined with and without forcing through the terrestrial composition.

			without forced intercept		with forced intercept	
Sample	Date		$^{60}Fe/^{56}Fe$ x10^{-7} (2 *)	MSWD	$^{60}Fe/^{56}Fe$ x10^{-7} (2 *)	MSWD
SMK DAP-1	**2010 July**	**RP**	**0.6 ± 1.5**	**11**	**0.5 ± 1.2**	**11**
SMK DAP-1	2011 Sept		0.7 ± 2.5	16	3.8 ± 1.5	23
SMK1805-5	2010 Dec	CC	*1.2 ± 3.4*	4	*-1.0 ± 2.2*	5
SMK 1805-5	2010 July		*-3.2 ± 2.6*	5	*0.5 ± 1.1*	12
SMK DAP-2	2011 July		*-0.2 ± 1.8*	7	*0.1 ± 1.1*	7
SMK MT r1	2012 Nov	PP	*1.4 ± 7.4*	4	*0.4 ± 2.5*	3
SMK312 chE mono*	2014 June	PO	*-2.9 ± 4.2*	7	*-1.0 ± 2.2*	7
SMK312 chQ mono	2014 June	POP	*-4.2 ± 10.0*	4	*-3.1 ± 3.0*	4
SMK312 chT mono	2014 June	POP	*-3.7 ± 4.5*	6	*-1.6 ± 1.7*	6
QUE 3*	**2013 June**	**BP**	**1.0 ± 4.5**	**5**	**0.6 ± 2.4**	**5**
QUE 3 mono	2014 June		*-2.1 ± 3.0*	4	*-0.9 ± 3.5*	7
QUE chI	2012 Nov	POP	*-0.1 ± 2.0*	3	*-2.7 ± 1.5*	5
QUE chK	2012 Nov	POP	*-0.9 ± 4.3*	1	*-0.9 ± 1.5*	1
QUE ch C*	2011 July	CC	*0.3 ± 8.3*	17	*-0.1 ± 7.4*	13
QUE chF	2011 July	BP	*0.2 ± 4.1*	21	*0.8 ± 1.7*	17
QUE 13 ch6	2011 April	POP	*-0.7 ± 1.6*	11	*-0.4 ± 0.7*	11
EET-r1	2012 Nov	POP	0.0 ± 1.1	14	-0.8 ± 0.8	17
BM80 ch13	**2010 Sept**	**POP**	**4.7 ± 9.5**	**23**	**4.9 ± 4.4**	**20**
BM80 ch37 multi*	2010 Sept	RP	*-2.1 ± 1.7*	*3*	*1.2 ± 2.2*	*3*
BM80 ch37 mono	**2010 Sept**		**2.4 ± 4.6**	**24**	**3.1 ± 3.0**	**24**
BM80 r40	2012 Nov	POP	*1.0 ± 7.8*	*12*	*-3.3 ± 2.2*	*12*
BM23 ch13*	2011 Sept	RP	*0.3 ± 2.3*	*4*	*-0.4 ± 0.9*	*4*
BM23 ch9	2011 April	POP	*0.1 ± 1.9*	*8*	*-0.4 ± 0.7*	*8*
BM23 ch12	2011 April	POP	*-1.2 ± 2.2*	*11*	*-1.4 ± 1.2*	*9*
BVG ch1	2010 Dec	BP	*1.2 ± 3.1*	*10*	*-0.9 ± 1.9*	*13*
KRM94 ch1	2011 Sept	CC	-1.0 ± 1.4	11	-0.2 ± 0.5	11
KRM93 ch 1	2011 July	RP	*0.8 ± 0.7*	*0*	*-0.2 ± 0.1*	*2*
KRM93 ch11	**2011 July**	**RP**	**1.5 ± 8.6**	**4**	**1.7 ± 0.6**	**3**
KRM93 ch11	**2008 Dec**		**1.7 ± 1.6**	**12**	**2.3 ± 0.9**	**12**

Chondrules that have consistent results regardless of whether the intercept is forced through terrestrial are highlighted in grey. [a]Isoplot gives the 95% confidence error when the probability of fit is very low < 15%. RP = radial pyroxene, CC = cryptocrystalline chondrule, PP = porphyritic pyroxene, PO = porphyritic olivine, POP = porphyritic olivine pyroxene, BP = barred pyroxene, BO = barred olivine. *These chondrules show evidence for interference contribution that is higher than the 1‰ contribution determined for most chondrules.

to optimize the gain of the detectors at the beginning of each SIMS session. We made no further adjustments during the day. We analyzed standards several times to characterize the gains at the beginning of the measurement session. Then we measure the standards throughout each day and use sample-standard bracketing to monitor and correct for drift in the gains of the detectors.

Molecular interferences: To resolve major molecular interferences on the Ni isotopes (*e.g.*, $^{44}Ca^{16}O$ on ^{60}Ni, $^{45}Sc^{16}O$ on ^{61}Ni, and $^{46}Ca^{16}O$ on ^{62}Ni), a mass resolving

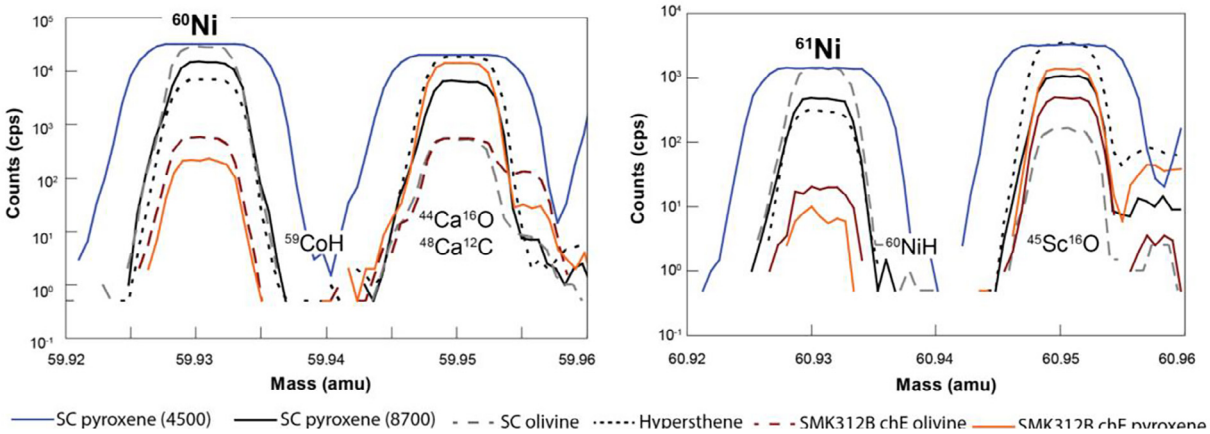

Fig. 1. Mass scans of ^{60}Ni and ^{61}Ni isotopes and interferences on San Carlos pyroxene and olivine and hypersthene terrestrial standards and also on Semarkona chondrule olivine and pyroxene grains (SMK312B chE). The mass scan for SC pyroxene is shown with mass resolving powers of 4500 and 8700. All other scans have MRPs of 8700. Major interferences (including $^{30}Si_2$, ^{46}TiO and others, which are not labeled here) are resolved with MRP of 4500 and interferences from ^{59}CoH on ^{60}Ni and ^{60}NiH on ^{61}Ni contribute less than 1‰ (refer to the on-line supplementary files for more details).

power (MRP) of ~4500 was used during multicollection analyses and a MRP of 6000–7000 was used during monocollection analyses. However, this does not resolve the ^{60}Ni hydride on ^{61}Ni (requires MRP = 8124). To evaluate the influence of ^{60}NiH on ^{61}Ni, we carried out high-resolution scans with MRPs >8000 during each SIMS session. We consistently found the ^{60}NiH peak and other hydrides (e.g., ^{59}CoH on ^{60}Ni and ^{61}NiH on ^{62}Ni) to contribute less than 1‰ to the Ni isotopes for both standards and samples (e.g., Fig. 1 and on-line supplementary files). Interferences were often measured during each measurement (via peak jumping) or after each measurement (by deflecting the secondary beam). We also tried to address the possible influence of unresolved complex molecular interferences on our analyses, such as the $[^{56}Fe^{64}Zn]^{2+}$ interference on ^{60}Ni (resolved with MRP = 47,190). Similar to Mishra and Goswami (2014), we did not find any significant counts associated with complex molecular interferences. The contribution of tails of the interferences on the Ni peaks is discussed in Section 2.3.

Uncertainties in the relative sensitivity factor ($^{56}Fe/^{61}Ni_{true}/^{56}Fe^{+}/^{61}Ni^{+}_{measured}$) can stem from using different beam currents for the standards and samples or using non-matrix-matched standards. The Fe and Ni content of chondrule pyroxene compositions range from 4 to 7 at.% and <0.01 at.% respectively. The Fe and Ni content for our synthetic standard and hypersthene standard are very similar to those of our chondrules, but we often use San Carlos pyroxene, which has an Fe content of 1.7 at.% and Ni of 0.03 at.%, quite different from our samples. To deal with the different sensitivity factors, we apply a relative sensitivity factor correction to the Fe/Ni ratios. The Fe/Ni ratio varies with time during a SIMS measurement. This can result in variations in the relative sensitivity factor depending on the length of the measurements. To account for this, we measure standards and samples for the same amount of time, even though we do not require all the cycles to get the precision we need on the standards.

2.3. Data analysis

Calculating isotope ratios from counting data results in a positive bias that correlates inversely with the number of counts of the normalizing isotope (Ogliore et al., 2011). Calculating ratios by averaging the ratios from the measurement cycles makes this problem worse because a cycle has fewer counts than the total measurement. The measured Fe/Ni ratios vary by up to one order of magnitude. Because the Fe concentration varies by only a few percent, the variation in Fe/Ni ratio is almost entirely due to the Ni concentration. Thus, the higher the Fe/Ni ratio, the lower the Ni counts and the greater the bias in the Ni-isotope ratio. This produces a correlation on an isotope plot that resembles an isochron. Ratio bias propagates into the slope of the isochron in different ways depending on how the data are reduced. For the ^{60}Fe-^{60}Ni system, an internal mass-fractionation correction using biased ratios produces a positive bias in the slope of the isochron when normalizing with ^{61}Ni, or a small negative bias in the slope when normalizing with ^{62}Ni (Telus et al., 2012). In order to significantly reduce the effect of ratio bias, isotope ratios reported here were calculated from total counts, a less-biased method of calculating ratios (Ogliore et al., 2011). This method involves summing the counts of the numerator isotope over all cycles and dividing by the summed counts of the denominator isotope over all cycles (time interpolation is done for monocollection to account for the differences in count times of the different isotopes). To further ensure that ratio bias is not an issue, we check that the data normalized to ^{61}Ni and ^{62}Ni, which differ in abundance by a factor of ~3, are consistent.

Since we collected the data in cycles, we were able to include time interpolation and remove anomalous cycles due to spikes in the detector signal from Ni-rich phases, electronic noise, or primary beam dropout. The data were corrected for electron multiplier background (typically measured overnight at the end of the session for 5–10 h

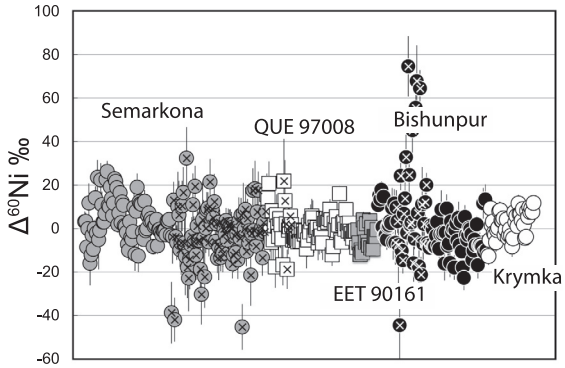

Fig. 2. Excess in ^{60}Ni for each spot analysis from each chondrite analyzed in this study. The superimposed crosses indicate analyses done in monocollection mode, all others were measured in multicollection mode. Errors are 2σ.

without the primary beam) and electron multiplier deadtime. Drift in the electron multiplier gain was corrected using sample-standard bracketing. Extraneous counts on the Ni peaks from the tails of interferences were determined using the tail-to-peak ratio ($\sim 1 \times 10^{-5}$), which was determined from measuring counts at the Ni peaks and counts at a few points along the tails, to the low-mass side of each peak (see on-line supplementary files). Contributions of tails of interferences onto Ni isotope counts are typically less than 1‰. However, chondrules QUE chC, SMK312B chE, BM23 ch13, BM23 ch37 (multicollection), and QUE ch3 (July 2013) show evidence for interference contributions that are higher than typical values (up to 5‰). Interference corrections were applied for these chondrules (except for SMK312B chE) and are provided in the supplementary files. The interference correction did not make a significant difference in the inferred initial ratio for these chondrules and are not used for the initial ratios reported in Table 1.

Uncertainties on the measured ratios include the standard error of the ratios calculated from individual cycles and uncertainties propagated from standard-sample bracketing. This allows us to account for non-statistical cycle-to-cycle variations during each measurement. To calculate excess in ^{60}Ni, we applied a linear internal mass-fractionation correction ($\Delta^{60}Ni = \delta^{60}Ni - 2 \times \delta^{61}Ni$ or $\Delta^{60}Ni = \delta^{60}Ni + \delta^{62}Ni$). Reference values of 7.215007 and 0.313629 were used for ^{60}Ni/^{61}Ni and ^{62}Ni/^{61}Ni, respectively (Gramlich et al., 1989). Mass-fractionation-corrected Δ^{60}Ni values are converted back to ratios for the isochron plots below using the same reference. Relative sensitivity factors ($^{56}Fe/^{62}Ni_{true}/^{56}Fe^{+}/^{62}Ni^{+}_{measured}$) for the ^{56}Fe/^{62}Ni ratios for olivine and pyroxene were applied based on the $^{56}Fe^{+}/^{62}Ni^{+}$ ratios of standards (San Carlos olivine, San Carlos pyroxene, hypersthene, or synthetic pyroxene) measured by SIMS and the Fe/Ni ratios measured by electron microprobe. The quoted uncertainties on the Fe/Ni ratios are dominated by the uncertainty on the sensitivity factor and are given as 5% of the measured ratios. The final uncertainty on the isotope ratios is corrected for the correlated component in the Ni-isotope ratios.

Using Isoplot Model 1 fit, the initial ^{60}Fe/^{56}Fe ratio for each chondrule is inferred from the error-weighted regression of ^{60}Ni/^{62}Ni (or ^{60}Ni/^{61}Ni) vs. ^{56}Fe/^{62}Ni (or ^{56}Fe/^{61}Ni). Uncertainties on the isochron slopes are reported as 2σ, or as 95% confidence errors when the probability of fit is less than 15% (or MSWD is very large). For each isochron, we report the mean square weighted deviation (MSWD), which characterizes how well the data fit the regression. The MSWD is the same as the reduced Chi squared; the term historically used for this parameter in statistics. Well-correlated regressions will have MSWDs close to 1. Detailed calculations for the data analyses are provided in the supplementary file for each chondrule.

3. RESULTS

3.1. Δ^{60}Ni values

The ^{61}Ni- and ^{62}Ni-normalized Ni isotope ratios and the Fe/Ni ratios for each chondrule analyzed in this study are provided in the on-line supplementary material. Fig. 2 shows the Δ^{60}Ni values for each spot analysis from each chondrule reported here. There is considerable scatter in the data, but most are indistinguishable from zero. Of the 24 chondrules analyzed for this study, a few chondrules have resolved excesses in ^{60}Ni of up to ~70‰. Negative values were determined for some spot analyses. Many of the highly negative values were obtained by monocollection. In the following section, we determine which chondrules provide the best constraints on the initial ^{60}Fe/^{56}Fe ratio of UOCs.

3.2. Initial ^{60}Fe/^{56}Fe ratio of UOC chondrules

It is important to calculate the initial ratios using both the ^{61}Ni and ^{62}Ni normalization to monitor the extent of ratio bias, which propagates into the isochron differently depending on how the mass-fractionation correction is made and depending on which normalizing isotope is used (Telus et al., 2012). An internal mass-fractionation of biased ratios using ^{62}Ni/^{61}Ni results in under-correcting the ^{60}Ni/^{61}Ni ratios and introducing a positive bias in the inferred initial ratio. When the ^{62}Ni normalization is used instead, an internal mass-fractionation correction results in over-correcting the ^{60}Ni/^{62}Ni ratios, producing a negative bias in the initial ratio. Also, since ^{62}Ni has more counts, using it as the normalizing isotope generally gives results that are less biased. When the ratios are calculated by summing the counts from all cycles of a measurement instead of averaging the ratios from each cycle (Ogliore et al., 2011), the choice of normalizing isotope for the nickel isotope ratios (^{61}Ni or ^{62}Ni) does not change the result. However, the uncertainty for ratios normalized to ^{62}Ni is systematically larger than for ratios normalized to ^{61}Ni due to the internal mass-fractionation correction (the uncertainty on the ^{61}Ni/^{62}Ni ratio is multiplied by 2). Initial ratios determined from ratios normalized to ^{61}Ni and ^{62}Ni are consistent (see supplementary files). For the rest of this paper, we refer only to ^{62}Ni-normalized ratios.

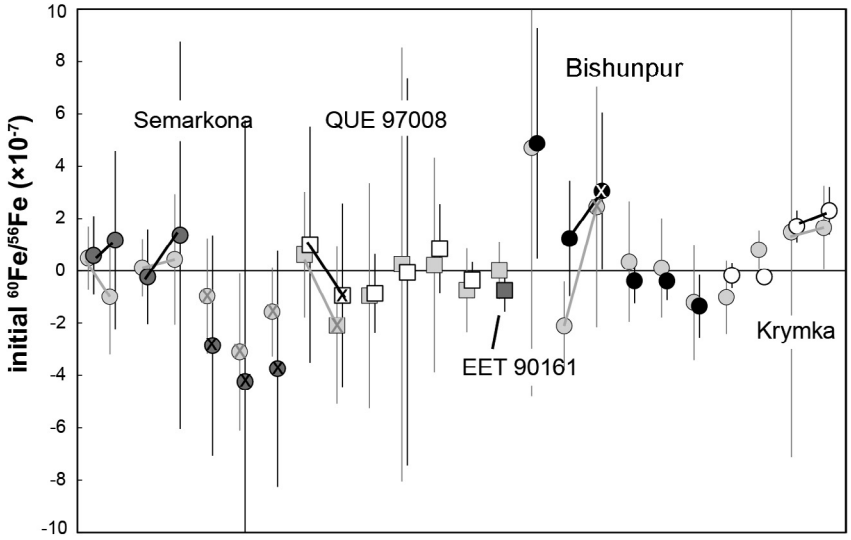

Fig. 3. Initial $^{60}Fe/^{56}Fe$ ratios of UOC chondrules determined without forcing the intercept (solid symbols) and with forcing the intercept (light grey symbols). Points with crosses were measured in monocollection mode, while all others were analyzed in multicollection mode (see Section 2 for details). Tie lines indicate analyses for the same chondrule but different analytical sessions.

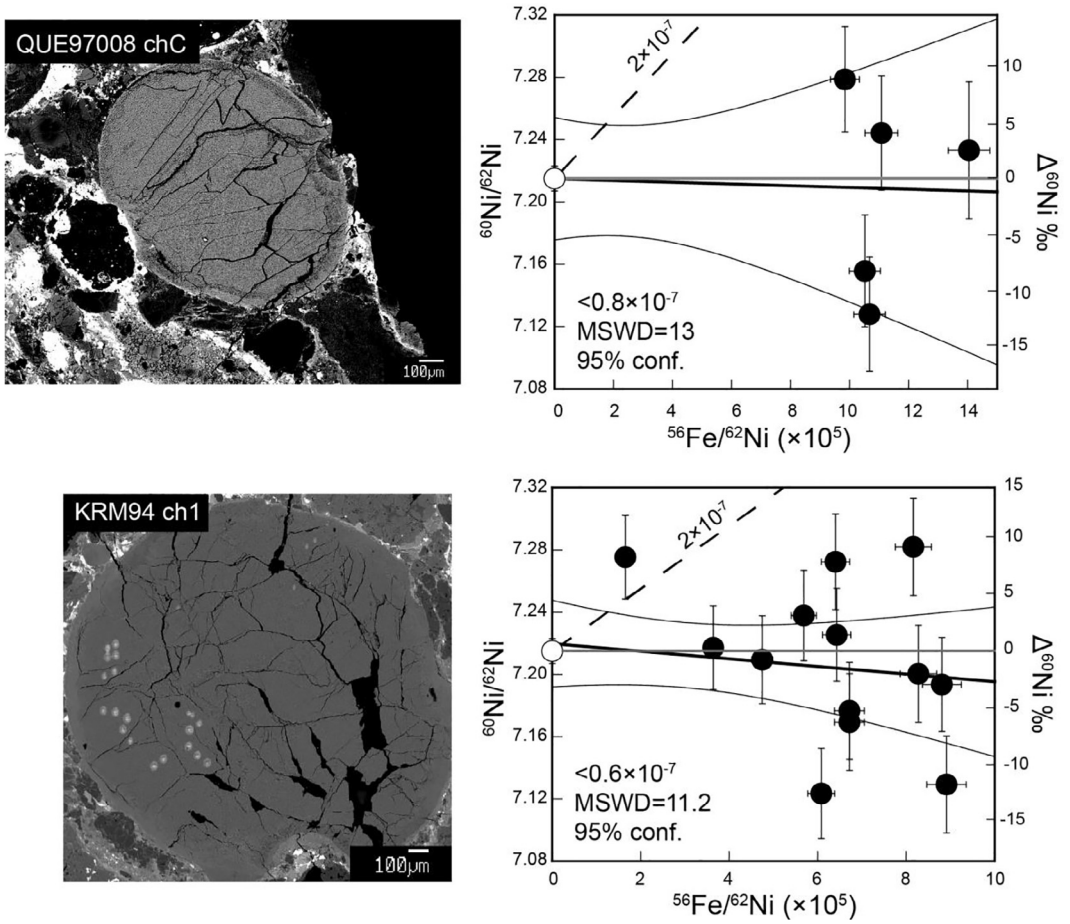

Fig. 4. Backscattered electron image and model isochrons for QUE 97008 chondrule chC (top) and Krymka chondrule KRM94 ch1 (bottom). The Y-axis is the fractionation-corrected $^{60}Ni/^{62}Ni$ ratios (left) and the excess in ^{60}Ni in permil (right). Despite the high Fe/Ni, the inferred initial ratios are unresolved from zero. The fine lines mark the error envelope and the grey horizontal line marks the terrestrial $^{60}Ni/^{62}Ni$ composition.

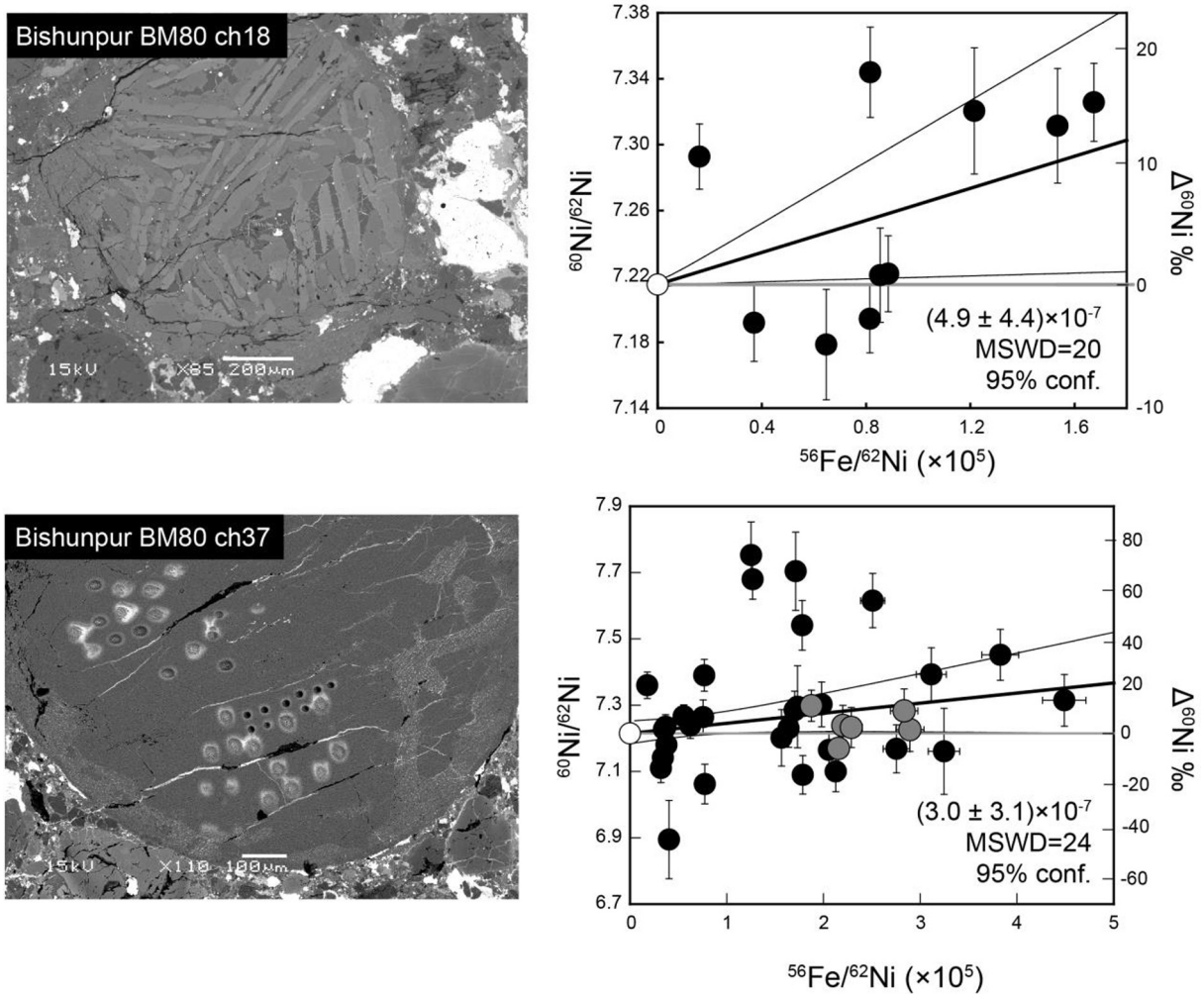

Fig. 5. Backscattered electron image and model isochron for Bishunpur chondrules BM80 ch13 and ch37. BM80 ch37 was analyzed in monocollection mode (black circles) and in multicollection mode (grey circles).

To determine which chondrules provide the best constraints, we determined the initial ratio in two ways: with and without forcing the regression through the terrestrial composition (*e.g.*, $^{56}Fe/^{62}Ni = 0.001 \pm 0.001$ and $^{60}Ni/^{62}Ni = 7.215 \pm 0.005$). The initial ratios are summarized in Table 1 and Fig. 3. Several chondrules have results that differ significantly when the intercept is forced through the terrestrial composition. This includes SMK DAP1 (Sept. 2011), SMK 1805-5 (July 2010), SMK312B chE, SMK312B chT, QUE chI, BM80 ch37 multi, BM80 r40, and BVG ch1. In some cases, the large difference between the inferred initial ratios is due to a limited range in the Fe/Ni and/or the Ni-isotope ratios (*e.g.*, SMK 1805-5 (July 2010), SMK312B chE, SMK312B chT, BM80 r40, and BM80 ch37 multi). For these datasets, the slope is better constrained when the intercept is forced through terrestrial. However, the inconsistencies in the inferred initial ratio for SMK DAP1 (Sept. 2011), QUE chI, and BVG ch1 are due to large positive or negative offsets in the Ni-isotopic composition of the chondrules from terrestrial. For instance, spot analyses for SMK DAP1 (Sept. 2011) have Ni-isotopic compositions that are significantly higher than the terrestrial composition that was not observed for previous sessions (*e.g.*, SMK DAP-1 (July 2010)). The difference between sessions may be due to differences in the analytical methods (*e.g.*, smaller spot size), but we cannot say for certain why there is this difference. Spot analyses for chondrules QUE chI and BVG ch1 have Ni-isotopic compositions that are much lower than the terrestrial standards.

Many chondrules have essentially the same initial ratio regardless of how the isochron is determined. Most of these are indistinguishable from zero, including SMK DAP1 (July 2010), SMK DAP2, SMKMT r1, SMK312 chQ, QUE ch3, QUE chK, QUE chC, QUE chF, QUE ch6, EET r1, BM23 ch13, BM23 ch9, BM23 ch12, and KRM94 ch1. A few of these chondrules have resolved initial ratios. Bishunpur chondrules, BM80 ch13 and BM80 ch37, have a resolved initial ratio of $(4.9 \pm 4.4) \times 10^{-7}$ and $(3.1 \pm 3.0) \times 10^{-7}$, respectively when the intercepts are forced through terrestrial. With the large scatter in the $^{60}Ni/^{62}Ni$ ratios and the very large MSWD of 20 and

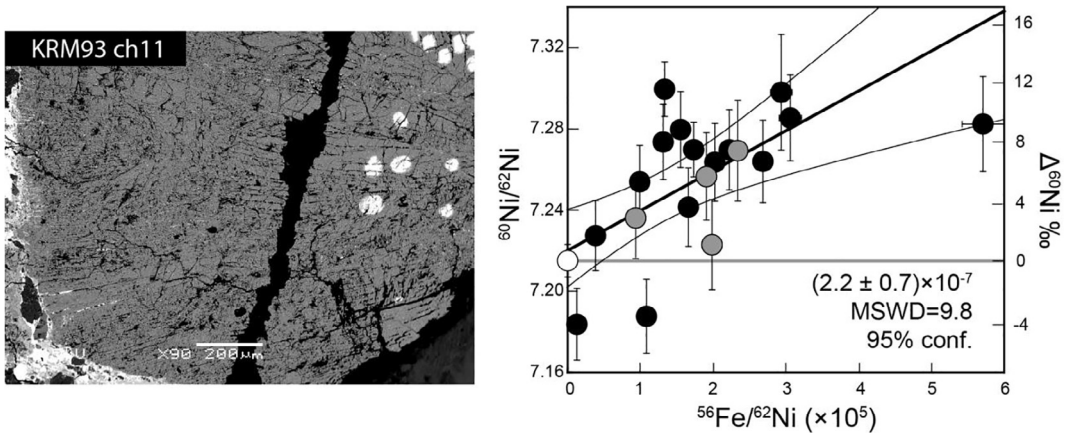

Fig. 6. Backscattered electron image and model isochron for Krymka chondrule KRM93 ch11. This chondrule was analyzed on two different occasions (black symbols are from Dec 2008 and grey symbols are from July 2011 analyses). The initial ratio inferred from the combined dataset is $(2.2 \pm 0.7) \times 10^{-7}$ with an MSWD of 10.

24, it is clear the Fe-Ni systematics of these chondrules have been disturbed. Krymka radial pyroxene chondrule, KRM93 ch11, consistently gives a resolved initial ratio of 2.0×10^{-7} from two different datasets, regardless of whether the intercept is forced through terrestrial. Details for each dataset are available in the supplementary information.

3.3. Chondrules with unresolved initial ratios, despite high Fe/Ni ratios

Some of our chondrules have very high Fe/Ni, but do not show evidence for excess ^{60}Ni. For example, QUE97008 chC and Krymka chondrule KRM94 ch1 are large cryptocrystalline chondrules with high Fe/Ni ($>1 \times 10^6$), but the inferred initial ratios are unresolved from zero (Fig. 4). With such high Fe/Ni and uncertainties of ~5‰ on Δ^{60}Ni, an initial ratio $>1 \times 10^{-7}$ should be easily resolved.

3.4. Chondrules with resolved initial ^{60}Fe/^{56}Fe ratios

The data for Bishunpur chondrule BM80 ch13, a porphyritic olivine-pyroxene chondrule, gives an initial ratio of $(4.9 \pm 4.4) \times 10^{-7}$ with an MSWD of 20 when the intercept is forced through the terrestrial composition (Fig. 5). The initial ratio is similar without the forced intercept, except the uncertainty is much larger. Bishunpur BM80 ch37 is a large (>1 mm) cryptocrystalline pyroxene chondrule. The initial ratio inferred from the monocollection data set is $(3.0 \pm 3.1) \times 10^{-7}$ with an MSWD of 24 when the intercept is forced through the terrestrial composition (Fig. 5). It is heavily bleached, but we avoided the obviously bleached zones. This chondrule was analyzed in two different modes, monocollection mode (black circles) and multicollection mode (grey circles). The monocollection data are more scattered than the multicollection analyses. Many monocollection spot analyses exhibit large positive values for Δ^{60}Ni (up to 70‰), but also large negative values (up to −40‰). The ^{56}Fe/^{62}Ni span a wide range for the monocollection data, while those for multicollection form a relatively tight cluster around 2.5×10^5. The scatter in the data for both of these chondrules is likely from Fe-Ni mobilization (see supplementary material in Telus et al., 2016).

Krymka chondrule KRM93 ch11 is a large (>1 mm) heavily fractured cryptocrystalline pyroxene chondrule (Fig. 6). Submicron sulfide blebs are also pervasive in this chondrule and were impossible to avoid for our spot analyses. We aimed to avoid large fractures but many of the fine fractures could not be avoided. This chondrule was analyzed on two separate occasions and the results are consistent (Table 1). When the intercept is forced through terrestrial, the inferred initial ratio from the July 2011 measurements is $(1.7 \pm 0.6) \times 10^{-7}$ and that for the December 2008 measurements is $(2.3 \pm 0.9) \times 10^{-7}$; combined, the initial ratio is $(2.2 \pm 0.7) \times 10^{-7}$ with an MSWD of 10.1 (Fig. 6). This chondrule appears to provide our strongest constraints on the initial ^{60}Fe/^{56}Fe ratio of UOC chondrules.

4. DISCUSSION

We have presented Fe-Ni SIMS data of UOC chondrules that were collected over the past several years. Most of the chondrules do not show resolved excesses in ^{60}Ni (Fig. 2). The initial ^{60}Fe/^{56}Fe for UOC chondrules inferred from our analyses are mostly unresolved (Table 1, Fig. 3), but a few show large excesses in ^{60}Ni and resolved initial ratios (Figs. 5 and 6). Here, we discuss complications from Fe-Ni redistribution on placing constraints on the initial ^{60}Fe/^{56}Fe ratio of UOC chondrules (Telus et al., 2016) and we place some constraints on the upper and lower limits of the initial ^{60}Fe/^{56}Fe ratio of UOC chondrules.

4.1. Complications from Fe-Ni mobilization in UOC chondrules

It is often assumed that olivine and especially pyroxene remained closed for Fe and Ni in chondrules from UOCs because volume diffusion of Ni in these phases should be

insignificant at the low peak temperatures experienced by these chondrites. However, Fe and Ni X-ray fluorescence maps presented by Telus et al. (2016) show clear evidence for extensive open-system Fe-Ni redistribution between UOC chondrules and the surrounding matrix. All UOCs regardless of petrologic type and regardless of whether fall or find show enrichment of Fe and/or Ni along chondrule fractures, with the finds showing the most extensive Fe-Ni mobilization. Fractures permeate the chondrules and their constituent minerals at all scales, making them difficult to avoid. The mobilization of Fe and Ni along chondrule fractures indicates that grain boundary diffusion and/or fluid transport is the dominant mechanism for Fe-Ni redistribution. The X-ray maps indicate that grain boundary diffusion and/or fluid transport can redistribute Fe and Ni over hundreds of microns. Late-stage and low-temperature exchange of Fe and Ni between chondrules and matrix was likely facilitated by aqueous alteration on the parent body and/or by terrestrial weathering.

Bulk Fe-Ni analyses of chondrules are especially vulnerable to this alteration because chondrule fractures cannot be avoided. For bulk analyses, extraneous Fe will increase the Fe/Ni ratios, resulting in points moving to the right on the isochron diagram and resulting in a lower inferred initial ratio. Extraneous Ni will decrease the Ni isotope ratios, moving points toward the intercept on the isochron diagram, but not necessarily changing the initial ratio. However, moving points toward the intercept can make excesses in ^{60}Ni difficult to resolve. Most likely, extraneous Fe and Ni are incorporated simultaneously during bulk analyses. This would move points down the isochron (from adding Ni) and to the right (from adding Fe), resulting in a lower inferred initial ratio (Telus et al., 2016). Attempts to alleviate this issue by leaching chondrules prior to chemical digestion may not remove all of the extraneous material and leaching may also result in removing Fe and Ni from the olivine and pyroxene grains themselves. Loss of Fe during leaching will move points to the left on the isochron diagram, while loss of Ni will move points to the right. If Ni is more readily leached than Fe (Quitté et al., 2011), then leaching will also result in lower inferred initial ratios as this produces artificially high Fe/Ni. Additionally, any incorporation of matrix material during sample preparation will result in lowering the inferred initial ratio.

In situ analyses that incorporate extraneous Fe will have higher Fe/Ni ratios, moving points to the right on the isochron diagram and resulting in lower inferred initial ratios. Incorporation of extraneous Ni will decrease Fe/Ni and decrease excess ^{60}Ni and move points toward the intercept along the original slope. Similar to results for bulk analyses, incorporating both extraneous Fe and Ni will result in lower inferred initial ratios. Extraneous Fe and Ni in chondrule fractures may not affect all spot analyses. If one could isolate only those measurements that did not incorporate extraneous Fe and Ni, reliable results could be obtained. But a mixture of "good" points and "bad" points will give poorly correlated isochrons (Telus et al., 2016). Also, lattice diffusion of Ni from olivine or pyroxene into sulfide or metal blebs can result in poorly correlated isochrons if some SIMS spots incorporate metal/sulfide blebs located within pyroxene grains, while others do not.

4.2. Interpretation of unresolved initial ratios

Our ability to resolve initial ratios using our *in situ* analyses is limited by the uncertainties on the Ni isotope ratios. Initial ratios $>2 \times 10^{-7}$ should be resolved with *in situ* analyses if Fe/Ni are sufficiently high. However, chondrules may not show resolved excesses in ^{60}Ni if they formed after a significant amount of ^{60}Fe had already decayed. For instance, if the initial solar system ^{60}Fe/^{56}Fe ratio was 2×10^{-7}, then chondrules that formed >2.6 Ma after solar system formation (i.e., after 1 half-life of ^{60}Fe) would have an initial ratio of $<1 \times 10^{-7}$, which we cannot always resolve with the current *in situ* techniques.

On the other hand, synchrotron maps from Telus et al. (2016) indicate that redistribution of Fe and Ni can result in lower inferred initial ratios. For example, Krymka chondrule KRM94 ch1 and QUE97008 chC have high ^{56}Fe/^{62}Ni ratios ($>1 \times 10^{6}$), but the inferred initial ^{60}Fe/^{56}Fe ratios are unresolved (Table 1, Fig. 4). Synchrotron XRF maps of KRM94 ch1 show extensive Fe-Ni mobilization along the chondrule fractures, with many of our spot analyses overlapping these fine fractures (see Fig. 11 in Telus et al., 2016). This indicates that the low initial ratio for this chondrule likely does not reflect its true initial ratio. Telus et al. (2016) also found that almost all chondrules from UOC finds show extensive Fe-Ni redistribution; thus, *in situ* analyses of chondrules from QUE 97008 and EET 90161 may also be compromised in this way. Bulk analyses of chondrules from finds (Tang and Dauphas, 2012a; Spivak-Birndorf et al., 2012a, 2012b) are also likely affected by extraneous Fe and Ni.

4.3. Estimating the lower limit on ^{60}Fe/^{56}Fe of the UOC chondrule-forming region

The observed excesses in ^{60}Ni and Fe/Ni can be used to place constraints on the initial ^{60}Fe/^{56}Fe. We find ^{60}Ni excesses up to ~70‰ (Fig. 5 and 6). The presence of excess ^{60}Ni of this magnitude in Fe-rich igneous objects indicates that the excesses come from the decay of ^{60}Fe. Nonradiogenic Ni isotope anomalies are not this large (e.g., Birck and Lugmair, 1988; Chen et al., 2009) and would have likely been reduced by mixing with normal Ni during the melting and crystallization that produced chondrules.

Redistribution of Fe and Ni can decrease Δ^{60}Ni, but it cannot increase them. Decreases in Δ^{60}Ni can be achieved by adding terrestrial Ni, while increasing Δ^{60}Ni would require additional input of only ^{60}Ni and not the other Ni isotopes, which is highly unlikely. Therefore, we can use the highest Δ^{60}Ni values of ~70‰ to help constrain the true initial ^{60}Fe/^{56}Fe ratios prior to Fe-Ni redistribution. Below, we discuss constraining the lower limit of the initial ^{60}Fe/^{56}Fe for UOC chondrules by determining the initial ratio consistent with the largest possible Fe/Ni and the largest Δ^{60}Ni values for UOC chondrules.

It is possible that the high initial ratios inferred from *in situ* analyses are a result of redistribution of Fe and Ni.

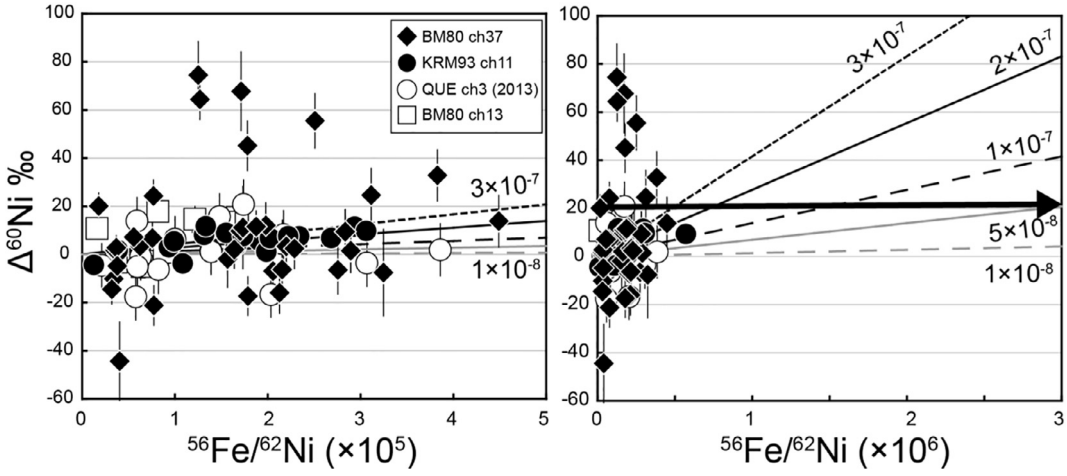

Fig. 7. Fe-Ni SIMS data for chondrules with resolved initial ratios. Here we assume that the measured excesses in ^{60}Ni provide a lower limit on the true excess since Δ^{60}Ni only decreases as a result of redistribution. Comparison of various initial ratios with this data illustrates that excesses in ^{60}Ni of 20‰ require initial ^{60}Fe/^{56}Fe ratios of at least 5×10^{-8} (right) given a maximum ^{56}Fe/^{62}Ni ratio of 3×10^6. This lower limit is determined by assuming the high initial ratios of chondrules were lower than what is inferred from the data due to Fe-Ni redistribution in chondrules. Since Δ^{60}Ni only decreases as a result of redistribution, we assume that the measured excesses in ^{60}Ni are a lower limit on the true excess. In order to have had a lower initial ratio, the Fe/Ni ratio was larger than what we measure. Assuming a maximum possible ^{56}Fe/^{62}Ni ratios of up to 3×10^6, an initial ratio of at least $\sim 5 \times 10^{-8}$ is required to produce excesses in ^{60}Ni ~20‰.

This could occur by decreasing Fe/Ni via preferential loss of Fe or by concentrating the radiogenic nickel in specific phases. This would mean that the Fe/Ni ratios during the decay of ^{60}Fe were higher than what we now observe. The maximum ^{56}Fe/^{62}Ni we have measured in our chondrules is $\sim 1 \times 10^6$ (*e.g.*, EET r1). Constraining the highest possible Fe/Ni prior to Fe-Ni redistribution is not straightforward, but we know that the initial Fe/Ni ratios of chondrule Fe-silicates cannot be infinitely large, since their values are limited by partitioning among phases. We have taken a ^{56}Fe/^{62}Ni ratio of 3×10^6 as an upper limit for the highest possible Fe/Ni ratio. This is significantly higher than what we have observed for any of our analyses.

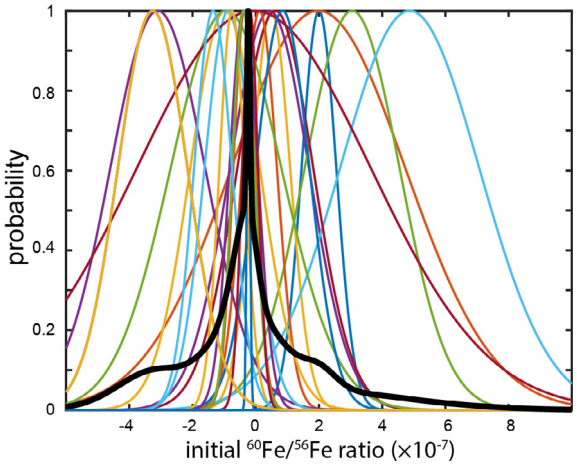

Fig. 8. Gaussian probability distributions for chondrules listed in Table 1 (color). The sum of the distributions, shown in black, has a one-sided upper limit of 3.0×10^{-7} (95% confidence) for the initial ^{60}Fe/^{56}Fe of UOC chondrules. This assumes these chondrules formed in a region where ^{60}Fe was distributed homogeneously. Data for SMKDAP-1 (Sept 2011), QUE chI, and BVG ch1 are not included in this calculation (see Results section for the explanation).

To constrain the lowest initial ^{60}Fe/^{56}Fe that could have produced the observed excesses in ^{60}Ni after FeNi redistribution, we use our estimate of the largest possible Fe/Ni together with the observed excesses in ^{60}Ni from chondrules with resolved initial ratios to place constraints on the initial ^{60}Fe/^{56}Fe of UOCs. Fig. 7 compares initial ratios from 1×10^{-8} to 3×10^{-7} with the data for chondrules with resolved initial ratios. In order to produce excess ^{60}Ni of 70‰, a lower limit on the initial ratio of 2×10^{-7} is required based on a maximum ^{56}Fe/^{62}Ni ratio of 3×10^6. However, only one chondrule (BM80 ch37 monocollection) has such large excesses in ^{60}Ni. Excesses of 20‰, observed for other chondrules, require a lower limit of 5×10^{-8}. The limitation of this exercise is that the value chosen for the Fe/Ni ratio prior to the assumed disturbance of the Fe-Ni system in the chondrule is unknown. If the Fe/Ni prior to the disturbance were significantly larger than our estimate of 3×10^6 for ^{56}Fe/^{62}Ni, this would result in an initial ^{60}Fe/^{56}Fe that is lower than our estimate. We do not have evidence for Fe/Ni in chondrules that are higher than our estimate.

Our estimate of 5×10^{-8} as the lower limit on the initial ^{60}Fe/^{56}Fe of UOC chondrules means that decreasing Fe/Ni by losing Fe or concentrating anomalous Ni can potentially produce excesses in ^{60}Ni of 20‰ provided that the true initial ratio was at least $\sim 5 \times 10^{-8}$. The mechanism for decreasing Fe/Ni is not clear, but may involve redistribution of Ni from pyroxenes into secondary metal/sulfide blebs during thermal metamorphism. *In situ* analyses of pyroxenes that include these secondary phases will have apparently low Fe/Ni, but relatively high Δ^{60}Ni values, moving points to the left on the isochron plot (see Fig. 13

in Telus et al., 2016). This has been reported for metal and chromite in the eucrite Juvinas (Quitté et al., 2011).

4.4. Probability distributions and upper limit on initial ratios for UOC chondrules

In Fig. 8, we sum the Gaussian distributions of the initial ratio for each chondrule listed in Table 1. As discussed earlier, open-system and closed-system alteration on a parent asteroid can potentially make higher or lower inferred $^{60}Fe/^{56}Fe$ ratios than the original values. However, these processes typically only lower ^{60}Ni excesses. If we assume that large ^{60}Ni excesses are more representative of the initial ^{60}Fe-^{60}Ni systematics of the objects, as is the case for ^{26}Al-^{26}Mg systematics of anorthite in some CAIs from metamorphosed chondrites (e.g., MacPherson et al., 1995), then the sum of the Gaussian distributions gives an upper limit on the initial $^{60}Fe/^{56}Fe$ ratios of the chondrules. We take the 95% confidence one-sided upper limit of this distribution of 3.0×10^{-7} as our best estimate of the upper limit on the initial $^{60}Fe/^{56}Fe$ ratio for UOC chondrules. However, averaging the initial ratios from numerous chondrules to determine the upper limit as done in Fig. 8 may not be valid if Fe and Ni redistribution occurred. This is difficult to constrain and may be higher than what is inferred from the sum the Gaussian distributions of the initial ratio for each chondrule.

4.5. Our best estimate of $^{60}Fe/^{56}Fe$ in the region where UOC chondrules formed

Due to complications from Fe-Ni mobilization, it is difficult to constrain the initial $^{60}Fe/^{56}Fe$ ratio of UOCs. An upper limit of 3.0×10^{-7} for UOC chondrules is estimated based on summing the Gaussian distributions of the inferred initial ratios (Figs. 8). We constrain the lower limit to be 5×10^{-8} based on excesses in ^{60}Ni of more than 20‰ from chondrules with resolved initial ratios (Fig. 7). This is a stronger constraint because the measured excess in ^{60}Ni cannot be explained if the initial ratio was significantly lower than this value. Previously reported *in situ* Fe-Ni systematics of UOC chondrules by Mishra and Goswami (2014) and Mishra and Chaussidon (2014) give higher initial ratios than the chondrules with resolved initial ratios reported in this study. Since these studies use similar analytical techniques, data analyses and samples, the apparent discrepancy between *in situ* analyses from this study and previous SIMS studies from Mishra remains unresolved.

4.6. Comparison with ICPMS and TIMS UOC chondrule data

Bulk analyses of chondrules from NWA5717 (UG3.05) and QUE97008 (L3.05) do not give resolved excess ^{60}Ni and do not show any correlation between excess ^{60}Ni and Fe/Ni (Tang and Dauphas, 2012a; Spivak-Birndorf et al., 2012a; Chen et al., 2013). Chondrules from Chainpur (LL3.4) also do not show resolved excess ^{60}Ni (Spivak-Birndorf et al., 2012b; Tang and Dauphas, 2012a); however, this is likely because this chondrite experienced significant thermal metamorphism with a peak temperature >400 °C (Huss and Lewis, 1994). The initial $^{60}Fe/^{56}Fe$ for UOCs inferred from these studies are all consistent with $<3 \times 10^{-8}$, inconsistent with initial ratios between 5×10^{-8} and 3.0×10^{-7} inferred from this study.

Tang and Dauphas (2015) focused their most recent bulk chondrule analyses on those from Semarkona because they show the least evidence for Fe-Ni mobilization. They analyzed 6 chondrules and found evidence for excess ^{60}Ni ($0.051 \pm 0.043\varepsilon$) in one, a Type II (Fe-rich) Semarkona chondrule. From their data, they infer an initial $^{60}Fe/^{56}Fe$ for UOCs of $(5.4 \pm 3.3) \times 10^{-9}$, consistent with the upper limit of $<3 \times 10^{-8}$ inferred from previous bulk chondrule studies. Based on preliminary results from synchrotron X-ray fluorescence mapping of UOC chondrules that found that 5 out of 16 (or 31%) of Semarkona chondrules were affected by Fe-Ni mobilization (abstract by Telus et al., 2013), Tang and Dauphas (2015) assume that most bulk analyses of Semarkona chondrules should be unaffected by Fe-Ni redistribution. However, additional synchrotron X-ray maps of Semarkona chondrules reported by Telus et al. (2016) show that 17 of 27 (or 63%) of chondrules from Semarkona exhibit clear evidence for Fe and/or Ni mobilization. Tang and Dauphas (2015) argue that parent-body disturbance will produce low Fe/Ni and that chondrules with high Fe/Ni should give reliable results. However, Telus et al. (2016) show that Fe-Ni mobilization introduces extraneous Fe and Ni into the chondrule which can increase the Fe/Ni ratio (by adding Fe) and move points toward the intercept (by adding Ni), resulting in artificially high Fe/Ni and low $\Delta^{60}Ni$ values and resulting in lower inferred initial $^{60}Fe/^{56}Fe$. Interestingly, chondrules with resolved initial ratios have $^{56}Fe/^{62}Ni$ of up to 5×10^5 (e.g., Figs. 5–7), while those with very high $^{56}Fe/^{62}Ni$ (up to 1×10^6) do not show evidence for excess ^{60}Ni (e.g., Fig. 4).

4.7. Coordinated bulk & *in situ* analyses of UOC chondrules

In collaboration with researchers at CalTech, we carried out coordinated bulk and *in situ* Fe-Ni analyses of chondrules from QUE97008 and Semarkona (QUE ch3 and SMKDAP-1). The bulk analyses were done using thermal ionization mass spectrometry and the results were reported by Chen et al. (2013). The chondrules were broken and fragments were reserved for *in situ* analysis. The chondrules were first washed in ethanol and HCl to remove metal or sulfide from the surface and in cracks. Then the chondrules were dissolved in strong acids. The Ni extraction procedures are described in Chen et al. (2009). Initial $^{60}Fe/^{56}Fe$ inferred from their bulk analyses are unresolved from zero, although a relatively high initial ratio of $\sim 1 \times 10^{-7}$ for QUE ch3 is permitted by the data (Chen et al., 2013). The *in situ* data for these chondrules are unresolved from terrestrial (Table 1). Additional studies involving coordinated bulk and *in situ* analyses are necessary to better understand the differences inferred from these two techniques.

4.8. Constraining the source of ^{60}Fe in the early solar system

4.8.1. Galactic background

An initial $^{60}Fe/^{56}Fe$ between 5×10^{-8} and 3.0×10^{-7} for UOCs corresponds to 8.5×10^{-8} and 5.1×10^{-7} for the initial Solar System $^{60}Fe/^{56}Fe$ ratio, $(^{60}Fe/^{56}Fe)_{SS}$, assuming all UOC chondrules formed 2 Ma after CAIs. Iron-60 in the early solar system could have been inherited from the galactic background, defined here (as in Huss et al., 2009) as the average composition of interstellar material from which molecular clouds form. Since SLRs have rapid decay rates, their abundance in the interstellar medium is generally low. The abundance of ^{60}Fe in the galactic background is constrained by comparing abundances determined from galactic chemical evolution models with the present day ^{60}Fe abundance in the galaxy determined from gamma-ray spectroscopic observations. With a galactic chemical evolution model to track the buildup of metals from when the galaxy formed (at 12 Ga) to when the solar system formed (at 4.6 Ga) and the present-day gamma ray emission fluxes of ^{60}Fe reported by Wang et al. (2007), the background $^{60}Fe/^{56}Fe$ ratio of $\sim 3 \times 10^{-8}$ is determined (see Eq. (14) in Huss et al., 2009). The lower limit of 0.8×10^{-7} inferred from out data is marginally above this estimate for galactic background, while our upper limit is well above this estimate. However, this comparison assumes that there is no additional delay time associated with isolating solar system material from the average galactic background (Clayton, 1983; Huss et al., 2009). The initial $^{60}Fe/^{56}Fe$ of the solar system inherited from the galactic background would be $\sim 10^{-9}$ when we consider that newly synthesized material requires 10–100 Ma to mix with the cold interstellar medium (McKee and Ostriker, 1977).

4.8.2. Single stellar sources

Injection of ^{60}Fe into the budding solar system from a single stellar source has been modeled for asymptotic giant branch (AGB) stars and type II supernovae (SNII). A single stellar source is defined here as a nearby (within a few parsecs) dying star that ejected material immediately prior to the solar system's formation. This mechanism has been considered a possible trigger for the collapse of the molecular cloud that formed the Solar System (Cameron and Truran, 1977; Boss and Keiser, 2010). During stellar nucleosynthesis, ^{60}Fe is produced via slow-neutron capture (s-process) on ^{59}Fe, which has a very short half-life of 44 days. For efficient production of ^{60}Fe, the neutron density must exceed $\sim$30 billion in order to get significant neutron capture on ^{59}Fe through s-process nucleosynthesis (Limongi and Chieffi, 2006). This requires temperatures between 4×10^8 and 2×10^9 degrees.

The high temperatures necessary for production of ^{60}Fe are achieved in the He shell of a 5 $M_\odot$ AGB star, where the $^{60}Fe/^{56}Fe$ is estimated to be $\sim 1 \times 10^{-6}$ (Wasserburg et al., 2006). Some ^{60}Fe production can occur through Cool Bottom Processing, which involves mixing material between the cool envelope and hotter and denser layers. Wasserburg et al. (2006) calculate initial $^{60}Fe/^{56}Fe$ of 4×10^{-8} to 2×10^{-7} for the envelopes of low mass AGB stars. The major drawback for an AGB source of ^{60}Fe is that these stars are old objects (relative to the lifetime of molecular clouds) and not associated with star formation regions (e.g., Kastner and Myers, 1994).

Massive stars between 11 $M_\odot$ and 33 $M_\odot$ die as type II supernovae. Nucleosynthesis models indicate that ^{60}Fe is produced copiously by massive stars (e.g., Limongi and Chieffi, 2006). Ejecta from a supernovae explosion could have potentially been incorporated during solar system formation. Presupernova, conditions for ^{60}Fe production are achieved during hydrostatic burning in the C and He burning shells (Limongi and Chieffi, 2006). Explosive nucleosynthesis of ^{60}Fe is most efficient when shock waves generated from the supernova pass through the C burning shell. The drawback for a supernova source of ^{60}Fe is that it produces excessive amounts of ^{53}Mn (e.g., Meyer, 2005). In order to better match the yields of supernova models and the initial $^{60}Fe/^{56}Fe$, $^{53}Mn/^{55}Mn$ and $^{26}Al/^{27}Al$ determined from isotope analyses, mixing at the C/O burning shell and fall back of a significant fraction of ejecta back onto the supernova remnant are required (Takigawa et al., 2008). A supernova source for ^{60}Fe is more likely than an AGB source because young stellar objects form in clusters where such massive stars are common (Williams and Gaidos, 2007). Wasserburg et al. (2006) calculate an initial $^{60}Fe/^{56}Fe$ of $\sim 2 \times 10^{-3}$ for the ejected stellar envelope of a 15 $M_\odot$ supernova source. The initial solar system $^{60}Fe/^{56}Fe$ inferred from our chondrule data is consistent with a single supernova as the source for ^{60}Fe. Nevertheless, some argue that a single supernova source is also unlikely because it is inconsistent with astronomical observations of star formation (e.g., Gounelle and Meynet, 2012; Young, 2014).

4.8.3. Self-enrichment of the molecular cloud

The solar system could have incorporated a $(^{60}Fe/^{56}Fe)_{SS}$ ratio higher than galactic background if it formed in a molecular cloud complex (i.e., a large molecular cloud that consists of multiple star clusters of different ages) that was enriched in ^{60}Fe. Here, we defined this process as self-enrichment (as in Huss et al., 2009); however, Gounelle and Meynet (2012) use "background" to refer to the same concept. Self-enrichment of the molecular cloud might occur if there was an enhanced abundance of ^{60}Fe from supernovae of multiple stars prior to the solar system's formation. Self-enrichment is preferred by Gounelle and Meynet (2012) because it provides a realistic mechanism for explaining the relative abundance of ^{26}Al and ^{60}Fe, which cannot be readily explained with a simple SN ejection. Gounelle and Meynet explain that $(^{60}Fe/^{56}Fe)_{SS}$ of $\sim 3 \times 10^{-7}$ and the $^{60}Fe/^{26}Al$ ratio can be explained if ^{60}Fe came from an older generation of massive stars within a giant molecular cloud ($\sim$15 Ma older), instead of one that died immediately before solar system formation. With our estimates of $(0.8–5) \times 10^{-7}$ for the initial Solar System ratio, $(^{60}Fe/^{56}Fe)_{SS}$, self-enrichment of the molecular cloud described here is possible and perhaps more likely than a single stellar source (Gounelle and Meynet, 2012).

In order to account for higher-than-background initial ratios of SLRs, Young (2014) incorporates the material ejected by winds from Wolf-Rayet stars, excluding the subsequent supernova explosion, into their GCE model since

these two ejections are separated in time. Winds from Wolf-Rayet stars have little effect on the ^{60}Fe abundance (Arnould et al., 2006). Young (2014) try to match the low initial ^{60}Fe/^{56}Fe inferred from bulk measurements, not those inferred from *in situ* analyses. Estimates of the initial ratio inferred from *in situ* analyses are not consistent with this model.

4.9. Developing the ^{60}Fe-^{60}Ni system for early solar system chronology

Constraining the initial ^{60}Fe/^{56}Fe of the Solar System is necessary for using the ^{60}Fe-^{60}Ni system for chronology. Although analytical issues from ratio bias have been addressed (Telus et al., 2012), discrepancies between *in situ* and bulk analyses of UOC chondrules remain. Late-stage open-system redistribution of Fe and Ni was prevalent and provides some explanation for these discrepancies (Telus et al., 2016). This alteration can easily compromise both the bulk and *in situ* analyses, resulting in either low inferred initial ratios or poorly correlated isochrons. Given the complications with Fe-Ni redistribution, UOCs may not be appropriate samples for constraining the initial Solar System ^{60}Fe/^{56}Fe ratio.

Our best approach in moving forward with ^{60}Fe-^{60}Ni analyses is to make a greater effort in identifying suitable samples prior to isotope analyses. For now, it is not clear which samples have escaped late-stage, low-temperature Fe-Ni mobilization. At least 60% of chondrules from Semarkona, the least metamorphosed ordinary chondrite, show evidence for this alteration. Although this is the least amount observed for any UOC, it still indicates that the majority of these chondrules have been compromised. *In situ* analyses can potentially avoid extraneous Fe-Ni in chondrule fractures if samples are thoroughly characterized. Bulk analyses must also take special precaution to avoid or remove contamination. However, with the pervasiveness of the remobilized Fe and Ni, this may not be possible.

Synchrotron X-ray fluorescence analyses provide the sensitivity, resolution, and efficiency for analyzing the distribution of Fe and Ni, at least in regards to Fe-Ni enrichment along chondrule fractures. Another benefit to synchrotron analyses is that they provide subsurface information of Fe and Ni distribution, which is not readily available from electron microscopy. Iron-Ni redistribution in chondrules from other chondrite groups (e.g., CO3 s) should also be investigated to determine if they could provide better constraints. Finally, synchrotron analyses of other important samples such as angrites and eucrites, which have been used to constrain the initial ^{60}Fe/^{56}Fe solar system ratio, should also be carried out.

5. CONCLUSIONS

To constrain the initial ^{60}Fe/^{56}Fe of the Solar System, we used the ion microprobe to measure ^{60}Fe-^{60}Ni systematics *in situ* in chondrule olivine and pyroxene in unequilibrated ordinary chondrites (UOCs). Most chondrules do not have resolved excesses in ^{60}Ni. Four chondrules show clearly resolved excesses in ^{60}Ni, but they do not correlate well with the Fe/Ni ratios as expected for a closed system and the initial ^{60}Fe/^{56}Fe ratios are poorly constrained (Table 1; Figs. 5 and 6). We use the excesses in ^{60}Ni determined from some our analyses to infer a lower limit of 5×10^{-8} for the initial ^{60}Fe/^{56}Fe ratio of the region where UOC chondrules formed (Fig. 7). The upper limit is more difficult to constrain due to complications from Fe-Ni redistribution, but we infer a value of 3.0×10^{-7} based on the upper limit of the sum of the probability distributions of each chondrule (Fig. 8). Initial ^{60}Fe/^{56}Fe ratios for UOCs between 5×10^{-8} and 3.0×10^{-7} are inconsistent with bulk analyses, which infer initial ratios of $< 3 \times 10^{-8}$ for UOC chondrules. The initial Solar System ^{60}Fe/^{56}Fe ratio of $(0.8–5)\times10^{-7}$ inferred from this study does not necessarily require a late supernova source for ^{60}Fe. Self-enrichment of the molecular cloud is another possible mechanism for incorporating ^{60}Fe in the solar system. Discrepancies between bulk and *in situ* analyses remain, but they likely stem from late-stage open-system Fe-Ni mobilization.

ACKNOWLEDGEMENTS

Thanks to Associate Editor, A. Davis and reviewers, N. Kita, and 1 anonymous reviewer, for extensive and helpful feedback on this paper. This work was supported by NASA NESSF grant NNX11AN62H, which supported the Ph. D. studies of M. Telus, and NNX11AG78G to G. R. Huss. Thanks to J. H. Chen and D. A. Papanastassiou for carrying out bulk TIMS analyses of UOC chondrules and for helpful comments on an early version of this manuscript. Thin sections of UOCs are from the Smithsonian Institution and the Meteorite Working Group. US Antarctic meteorite samples are recovered by the Antarctic Search for Meteorites (ANSMET) program, which has been funded by NSF and NASA, and characterized and curated by the Department of Mineral Sciences of the Smithsonian Institution and Astromaterials Curation Office at NASA Johnson Space Center. Thanks to J. E. Hammer for synthetic pyroxene standards. This is Hawai'i Institute of Geophysics and Planetology publication No. 2241 and School of Ocean and Earth Science and Technology publication No. 9878.

APPENDIX A. SUPPLEMENTARY MATERIAL

Supplementary data associated with this article can be found, in the online version, at http://dx.doi.org/10.1016/j.gca.2017.06.013.

REFERENCES

Arnould M., Goriely S. and Meynet G. (2006) The production of short-lived radionuclides by new non-rotating and rotating Wolf-Rayet model stars. *Astron. Astrophys.* **453**, 653–659.

Birck J. L. and Lugmair G. W. (1988) Nickel and chromium isotopes in Allende inclusions. *Earth. Planet. Sci. Lett.* **90**, 131–143.

Boss A. P. and Keiser S. A. (2010) Who pulled the trigger: a supernova or an asymptotic giant branch star? *Astrophys. J.* **717**, L1–L5.

Cameron A. G. W. and Truran J. W. (1977) The supernova trigger for formation of the solar system. *Icarus* **30**, 447.

Chen J. H., Papanastassiou D. A. and Wasserburg G. J. (2009) A search for nickel isotopic anomalies in iron meteorites and chondrites. *Geochim. Cosmochim. Acta.* **73**, 1461–1471.

Chen J. H., Papanastassiou D. A., Telus M. and Huss G. R. (2013) Fe-Ni isotopic systematics in UOC QUE97008 and Semarkona chondrules. *Lunar Planet. Sci.* **44**, #2649.

Clayton D. D. (1983) Extinct radioactivities – a three-phase mixing model. *Astrophys. J.* **268**, 381–384.

Gounelle M. and Meynet G. (2012) Solar system genealogy revealed by extinct short-lived radionuclides in meteorites. *Astron. Astrophy.* **545**, 4.

Gramlich J. W., Machlan L. A., Barnes I. L. and Paulsen P. J. (1989) Absolute isotopic abundance ratios and atomic weight of a reference sample of nickel. *J. Res. NIST* **94**, 347–356.

Guan Y., Huss G. R. and Leshin L. A. (2004) SIMS analyses of Mg, Cr, and Ni isotopes in primitive meteorites and short-lived radionuclides in the early solar system. *Appl. Surf. Sci.* **231–232**, 899–902.

Guan Y., Huss G. R. and Leshin L. A. (2007) ^{60}Fe-^{60}Ni and ^{53}Mn-^{53}Cr isotopic systems in sulfides from unequilibrated enstatite chondrites. *Geochim. Cosmochim. Acta* **71**, 4082–4091.

Hester J. J. and Desch S. J. (2005) Understanding our origins: star formation in HII region environments. *ASP Conf. Ser.* **341**, 107–127.

Huss G. R. and Lewis R. S. (1994) Noble gases in presolar diamonds II: component abundances reflect thermal processing. *Meteoritics* **29**, 811–829.

Huss G. R., Meyer B. S., Srinivasan G., Goswami J. N. and Sahipal S. (2009) Stellar sources of short-lived radionuclides in the early solar system. *Geochim. Cosmochim. Acta* **73**, 4922–4945.

Kastner J. H. and Myers P. C. (1994) An observational estimate of the probability of encounters between mass-losing evolved stars and molecular clouds. *Astrophys. J.* **421**, 605–614.

Kita N. T., Nagahara H., Togashi S. and Morishita Y. (2000) A short duration of chondrule formation in the solar nebula: Evidence from ^{26}Al in Semarkona ferromagnesian chondrules. *Geochim. Cosmochim. Acta* **64**, 3913–3922.

Limongi M. and Chieffi A. (2006) The nucleosynthesis of ^{26}Al and ^{60}Fe in solar metallicity stars extending in mass from 11 to120 $M_{\odot}$: the hydrostatic and explosive contributions. *Astrophys. J.* **647**, 483–500.

MacPherson G. J., Davis A. M. and Zinner E. K. (1995) The distribution of aluminum-26 in the early Solar System – a reappraisal. *Meteoritics* **30**, 365–386.

McKee C. F. and Ostriker J. P. (1977) A theory of the interstellar medium – three components regulated by supernova explosions in an inhomogeneous substrate. *Astrophys. J.* **218**, 148–169.

Mishra R. K., Goswami J. N., Tachibana S., Huss G. R. and Rudraswami N. G. (2010) Evidence in chondrules for contemporaneous injection of ^{26}Al and ^{60}Fe of stellar origin into the nascent solar system. *Astrophys. J.* **714**, L217–L221.

Mishra R. K. and Chaussidon M. (2014) Fossil record of high level of ^{60}Fe in chondrules from unequilibrated chondrites. *Earth. Planet. Sci. Lett.* **398**, 90–100.

Mishra R. K. and Goswami J. N. (2014) Fe–Ni and Al–Mg isotope records in UOC chondrules: plausible stellar source of ^{60}Fe and other short-lived nuclides in the early Solar System. *Geochim. Cosmochim. Acta* **132**, 440–457.

Moskovitz N. and Gaidos E. (2011) Differentiation of planetesimals and the thermal consequences of melt migration. *Meteorit. Planet. Sci.* **46**, 903–918.

Mostefauoi S., Lugmair G. W. and Hoppe P. (2005) ^{60}Fe: a heat source for planetary differentiation from a nearby supernova explosion. *Astrophys. J.* **625**, 271–277.

Ogliore R. C., Huss G. R. and Nagashima K. (2011) Ratio estimation in SIMS analysis. *Nucl. Instrum. Methods. Phys. Res. B* **269**, 1910–1918.

Ouellette N., Desch S. J., Bizzarro M., Boss A. P., Ciesla F. and Meyer B. (2009) Injection mechanisms of short-lived radionuclides and their homogenization. *Geochim. Cosmochim. Acta* **73**, 4946–4962.

Quitté G., Markowski A., Latkoczy C., Gabriel A. and Pack A. (2010) Iron-60 heterogeneity and incomplete isotope mixing in the early solar system. *Astrophys. J.* **720**, 1215–1224.

Quitté G., Latkoczy C., Schonbachler M., Halliday A. N. and Gunther D. (2011) ^{60}Fe-^{60}Ni systematics in the eucrite parent body: a case study of Bouvante and Juvinas. *Geochim. Cosmochim. Acta* **75**, 7698–7706.

Rugel G., Faestermann T., Knie K., Korschinek G., Poutivtsev M., Schumann D., Kivel N., Günther-Leopold I., Weinreich R. and Wohlmuther M. (2009) New measurement of the ^{60}Fe half-life. *Phys. Rev. Lett.* **103**, 072502.

Shukolyukov A. and Lugmair G. W. (1993a) Live Iron-60 in the early solar system. *Science* **259**, 1138–1142.

Shukolyukov A. and Lugmair G. W. (1993b) ^{60}Fe in eucrites. *Earth. Planet. Sci. Lett.* **119**, 159–166.

Spivak-Birndorf L. J., Wadhwa M. and Janney P. E. (2011) ^{60}Fe-^{60}Ni chronology of the D'Orbigny angrite: implications for the initial solar system abundance of ^{60}Fe. *Lunar Planet. Sci.* **42**, #2281.

Spivak-Birndorf L. J., Wadhwa M. and Janney P. E. (2012a) ^{60}Fe-^{60}Ni systematics of Chainpur chondrules and the plutonic angrites Northwest Africa 4590 and 4801. *Lunar Planet. Sci.* **43**, #2861.

Spivak-Birndorf L. J., Wadhwa M. and Janney P. E. (2012b) The ^{60}Fe-^{60}Ni systematics of chondrules from unequilibrated ordinary chondrites. *Meteorit. Planet. Sci.* **47**, A355.

Tachibana S. and Huss G. R. (2003) The initial abundance of ^{60}Fe in the solar system. *Astrophys. J.* **588**, L41–L44.

Tachibana S., Huss G. R., Kita N. T., Shimoda G. and Morishita Y. (2006) ^{60}Fe in chondrites: debris from a nearby supernova in the early solar system? *Astrophys. J.* **639**, L87–L90.

Tachibana S., Huss G. R. and Nagashima K. (2007) ^{60}Fe-^{60}Ni systems in ferromagnesian chondrules in least equilibrated ordinary chondrites. *Lunar Planet. Sci.* **38**, #1709.

Tachibana S., Huss G. R. and Nagashima K. (2009) Ion microprobe study of ^{60}Fe-^{60}Ni system in ferromagnesium pyroxene chondrules in Krymka (LL3.1) by multicollection. *Lunar Planet. Sci.* **40**, #1808.

Takigawa A., Miki J., Tachibana S., Huss G. R., Tominaga N., Umeda H. and Nomoto K. (2008) Injection of short-lived radionuclides from a faint mixing-fallback supernova into the early solar system. *Astrophys. J.* **688**, 1383–1387.

Tang H. and Dauphas N. (2012a) Abundance, distribution, and origin of ^{60}Fe in the solar protoplanetary disk. *Earth Planet. Sci. Lett.* **359–360**, 248–263.

Tang H. and Dauphas N. (2012b) Low abundance and homogeneous distribution of ^{60}Fe in the early solar system. *Lunar Planet. Sci.* **43**, #1703.

Tang H. and Dauphas N. (2015) Low ^{60}Fe abundance in Semarkona and Sahara 99555. *Astrophys. J.* **802**, 1–9.

Telus M., Huss G. R., Nagashima K., Ogliore R. C., Tachibana S. and Jilly C. E. (2011) Possible heterogeneity of 60Fe in chondrules from primitive ordinary chondrites. *Lunar Planet. Sci.* **42**, #2559.

Telus M., Huss G. R., Nagashima K., Ogliore R. C. and Tachibana S. (2012) Recalculation of data for short-lived radionuclide systems using less-biased ratio estimation. *Meteorit. Planet. Sci.* **47**, 2013–2030.

Telus M., Huss G. R., Nagashima K., Ogliore R. C., Chen J. H. and Papanasstassiou D. A. (2013) ^{60}Fe-^{60}Ni systematics of chondrules from UOC QUE 97008: comparing results from in situ and bulk analyses. *Meteorit. Planet. Sci.* **48**.

Telus M., Huss G. R., Ogliore R. C., Nagashima K., Howard D. L., Newville M. G. and Tomkins A. G. (2016) Mobility of iron and nickel at low temperatures and implications for ^{60}Fe-^{60}Ni systematics of chondrules from unequilibrated ordinary chondrites. *Geochim. Cosmochim. Acta* **178**, 87–105.

Wang W., Harris M. j., Diehl R., Halloin H., Cordier B., Strong A. W., Kretschmer K., Knödlseder J., Jean P., Lichti G. G., Roques J. P., Schanne S., von Kienlin A., Weidenspointener G. and Wunderer C. (2007) SPI observations of the diffuse ^{60}Fe emission in the galaxy. *Astron. Astrophys.* **469**, 1005–1012.

Wasserburg G. J., Busso M., Gallino R. and Nollett K. M. (2006) Short-lived nuclei in the early solar system: possible AGB sources. *Nucl. Phys. A* **777**, 5–69.

Williams J. P. and Gaidos E. (2007) On the likelihood of supernova enrichment of protoplanetary disks. *Astrophys. J.* **663**, L33–L36.

Young E. D. (2014) Inheritance of solar short- and long-lived radionuclides from molecular clouds and the unexceptional nature of the solar system. *Earth Planet. Sci. Lett.* **392**, 16–27.

Associate editor: Andrew M. Davis